MRI with and without a high-density EEG cap - what makes the difference?

Klein, Carina ; Hänggi, Jürgen ; Luechinger, Roger ; Jäncke, Lutz

Abstract: Besides the benefit of combining the imaging methods electroencephalography (EEG) and magnetic resonance imaging (MRI), much effort has been spent to develop algorithms aimed at successfully cleaning the EEG data from MRI-related gradient and ballistocardiological artefacts. However, previous studies have also shown a negative influence of the EEG on MRI data quality. Therefore, in the present study, we focussed for the first time on the influence of the EEG on morphometric measurements of T1-weighted MRI data (voxel- and surfaced-based morphometry). Our results delivered a strong influence of the EEG on cortical thickness, surface area, and volume as well as subcortical volumes due to local EEG-related inhomogeneities of the static magnetic (B0) and the gradient field (B1). In a second step, we analyzed the signal-to-noise ratios for both the anatomical and the functional data when recorded simultaneously with EEG and MRI and compared them to the ratios of the MRI data without simultaneous EEG measurements. These analyses revealed consistently lower signal-to-noise ratios for anatomical as well as functional MRI data during simultaneous EEG registration. In contrast, further analyses of T2*-weighted images provided reliable results independent of whether including the individuals' T1-weighted image with or without the EEG cap in the fMRI preprocessing stream. Based on our findings, we strongly recommend to not use the anatomical images obtained during simultaneous EEG-MRI recordings when there is an additional need or interest to focus on separate anatomical data analysis.

DOI: https://doi.org/10.1016/j.neuroimage.2014.11.053

MRI with and without a high-density EEG cap - what makes the difference?

Carina Klein, Jürgen Hänggi, Roger Luechinger, Lutz Jäncke

PII: S1053-8119(14)00983-5
DOI: doi: 10.1016/j.neuroimage.2014.11.053
Reference: YNIMG 11813

To appear in: *NeuroImage*

Accepted date: 26 November 2014

Please cite this article as: Klein, Carina, Hänggi, Jürgen, Luechinger, Roger, Jäncke, Lutz, MRI with and without a high-density EEG cap - what makes the difference?, *NeuroImage* (2014), doi: 10.1016/j.neuroimage.2014.11.053

MRI with and without a high-density EEG cap - what makes the difference?

Carina Klein[1§*], Jürgen Hänggi[1§], Roger Luechinger[2], and Lutz Jäncke[1,3-6]

[1] Division Neuropsychology, Institute of Psychology, University of Zurich, Switzerland

[2] Institute for Biomedical Engineering, University and ETH Zurich, Switzerland

[3] International Normal Aging and Plasticity Imaging Center (INAPIC), University of Zurich, Switzerland

[4] Center for Integrative Human Physiology (ZIHP), University of Zurich, Switzerland

[5] University Research Priority Program (URPP), Dynamic of Healthy Aging, University of Zurich, Switzerland

[6] Department of Special Education, King Abdulaziz University, Jeddah, Saudi Arabia

[§] These authors contributed equally to this work

* Corresponding author

Address for correspondence:

Carina Klein
Division Neuropsychology
Institute of Psychology
University of Zurich
Binzmuehlestrasse 14 / Box 25
CH-8050 Zurich, Switzerland
Tel.: +41 (44) 635 7557
Fax: +41 (44) 635 7409

Email addresses:

CK: c.klein@psychologie.uzh.ch

JH: j.haenggi@psychologie.uzh.ch

RL: luechinger@biomed.ee.ethz.ch

LJ: l.jaencke@psychologie.uzh.ch

Running head:

Simultaneous EEG net distorts MR images

Keywords:

Simultaneous EEG-fMRI, electroencephalography, functional and structural magnetic resonance imaging, MRI artefacts, magnetic susceptibility, eddy currents, chemical shift, SNR, distorted B_0 and B_1 map

Abstract

Besides the benefit of combining the imaging methods electroencephalography (EEG) and magnetic resonance imaging (MRI), much effort has been spent to develop algorithms aimed at successfully cleaning the EEG data from MRI-related gradient and ballistocardiological artefacts. However, previous studies have also shown a negative influence of the EEG on MRI data quality. Therefore, in the present study, we focussed for the first time on the influence of the EEG on morphometric measurements of T1-weighted MRI data (voxel- and surfaced-based morphometry). Our results delivered a strong influence of the EEG on cortical thickness, surface area, and volume as well as subcortical volumes due to local EEG-related inhomogeneities of the static magnetic (B_0) and the gradient field (B_1). In a second step, we analyzed the signal-to-noise ratios for both the anatomical and the functional data when recorded simultaneously with EEG and MRI and compared them to the ratios of the MRI data without simultaneous EEG measurements. These analyses revealed consistently lower signal-to-noise ratios for anatomical as well as functional MRI data during simultaneous EEG registration. In contrast, further analyses of T2*-weighted images provided reliable results independent of whether including the individuals' T1-weighted image with or without the EEG cap in the fMRI preprocessing stream. Based on our findings, we strongly recommend to not use the anatomical images obtained during simultaneous EEG-MRI recordings when there is an additional need or interest to focus on separate anatomical data analysis.

1. Introduction

Magnetic resonance imaging (MRI) techniques as well as electroencephalographic (EEG) measurements are well established and widely used in the field of clinical and cognitive neuroscience. To benefit from both the high spatial resolution of the MRI and the high temporal resolution of the EEG, bringing together these two imaging methods has gained increasing interest and advantages in the past few years. Much work has been done to develop algorithms aimed at successfully cleaning EEG data from MRI-related ballistocardiological and gradient artefacts (Herrmann and Debener, 2008; Ritter and Villringer, 2006). However, previous studies have shown that the EEG electrodes and even the composition of EEG equipment such as the electrode paste have a negative influence on MRI data quality (Bonmassar, 2001). In particular, the interaction of the magnetic field and the EEG channels lead to susceptibility artefacts, which create magnetic field inhomogeneities and hence cause a signal loss in the MRI data. In this context, Mullinger and colleagues (Mullinger et al., 2008) showed that an increasing number of electrodes (32 and 64 channel net) as well as an increasing magnetic field strength (1.5, 3, and 7 Tesla) lead to both B_0 and B_1 field perturbations that result in a decreasing signal intensity of the functional images in the affected regions. In addition, the strongest perturbations of the B_1, B_0, and the anatomical sequences were reported to be mainly driven by the electrocardiography (ECG) and the electrooculography (EOG) leads passing along the head (Mullinger et al., 2008).

Today, the usage of high-density EEG systems has become increasingly popular due to the benefit in source localization (Michel et al., 2004). Recently, Luo and Glover (Luo and Glover, 2012) tested the influence of a dense-array EEG system with 256 electrodes (the same system as used in the present study) on data quality of T2*-weighted functional and T2-weighted structural MRI sequences. Their findings reveal a significant reduction of the T2-weighted anatomical signal due to a shielding effect of the conducting wires, especially over

occipital regions where all the wires of the net come together. However, the signal-to-noise ratio (SNR) of the functional data with and without the EEG cap was comparable.

To the best of our knowledge, here we provide first evidence for the influence of a high-density EEG net on T1- and T2*-weighted (echo-planar) images at 3 Tesla. In particular, the influence of EEG electrodes on structural data analysis such as surface- and voxel-based morphometry was tested. In addition, B_0 and B_1 maps were recorded to examine whether a putative destructive effect on data quality arises from magnetic inhomogeneities of the static magnetic field or of perturbations of the radio frequency (RF) pulse. Furthermore, we tested whether including the individual T1-weighted image with and without the EEG cap in the spatial normalization step of the fMRI preprocessing has any influence on the localization of functional activity.

2. Methods

The present study is divided into a structural and functional part. In the structural part, the influence of a high-density EEG net (256 channels) on the quality of the T1-weighted magnetic resonance imaging (MRI) scans was investigated. First, we evaluated the influence of the EEG net on common morphometric features of T1-weighted MRI data such as cortical thickness and cortical surface area (derived from surface-based morphometry), subcortical volumes (derived from subcortical segmentations), as well as on voxel-wise probabilistic grey matter density (derived from voxel-based morphometry). Subsequently, we investigated the influence of the EEG net on the spatial signal-to-noise ratio (SNR) of the T1-weighted images, as well as on the homogeneity of the static magnetic (B_0) and the gradient field (B_1).

In the functional part of our study, the influence of the EEG net on the blood oxygenation level dependent (BOLD) signal was investigated, of both resting-state data as well as during a

simple auditory task. Here, we further assessed the influence of the EEG net on the temporal SNR. In addition, we also highlight the bias that is introduced into the spatial normalisation procedure of functional MRI scan time series when transformations are estimated based on the distorted T1-weighted image acquired while participants wore the EEG cap.

2.1 Subjects

Thirteen young subjects (seven women and six men) with a mean age of 28.2 years (standard deviation, SD = 3.02 years) participated in the structural part of the study. To evaluate any influence of T1-weighted images with and without the EEG cap on functional data, we recorded T2*-weighted images of 7 minutes resting state (without auditory stimulation, the control condition) with eyes open and a block of 6 minutes of auditory stimulation, the first movement of "A little night music" by W. A. Mozart) on six of the thirteen subjects from the T1 recordings (one man, five women) with mean age of 23.5 years, SD = 2.69 years. A functional T2*-weighted sequence (for a seed-based analysis of 5 minutes resting state data) and B_0 maps were recorded on five other subjects (one woman and four men with a mean age of 32.8 years, SD = 5.6 years). Five additional subjects (four women and one man with a mean age of 28 years, SD = 7.3 years) participated in the third part of data collection, with which the homogeneity of the B_1 field map was investigated. Except two men and one woman who participated in the T1 recordings, all other subjects were consistently right-handed as assessed by personal communication. Table 1 gives an overview about the recorded sequences and how many subjects were measured. Participants had no neurologic or psychiatric disease, showed no neuropsychological problems, and denied taking drugs or any illegal medication. The local ethics committee approved the study protocol and written informed consent was obtained from all participants.

Table 1. Overview of the recorded sequences / data processing and number of measured participants. Sequences that were applied to the same subjects are indicated with the same superscripts (either § or $^{\Delta}$). AC = auditory control condition; AS = auditory stimulation; DMN, default mode network; R = right handed; RS = resting state; RS-DMN = resting state data which were used for the seed based analysis of the DMN.

MR sequence	Number of subjects	Mean age ± SD	Number of women	Handedness
T1§	13	28.2 ± 3.02	7	10 R
T2* (AC, AS) §	6	23.5 ± 2.69	5	6 R
T2* (RS-DMN)$^{\Delta}$	5	32.8 ± 5.6	1	5 R
$B_0{}^{\Delta}$	5	32.8 ± 5.6	1	5 R
B_1	5	28 ± 7.3	4	5 R

2.2 Magnetic resonance imaging data acquisition

MRI scans were acquired on a 3.0 Tesla Philips Ingenia whole body scanner (Philips Medical Systems, Best, The Netherlands) equipped with a transmit-receive body coil and a commercial 15-element head coil array.

Two volumetric 3D T1-weighted gradient echo sequence (TFE, turbo field echo) scans were measured on 13 participants, one scan when participants wore the EEG cap and one scan without wearing the cap. The spatial resolution of these T1-weighted images was 1.0 x 1.0 x 1.0 mm^3 (acquisition matrix 240 × 240 pixels, 160 slices) and reconstructed to a resolution of 0.94 × 0.94 × 1.0 mm^3 (reconstruction matrix 256 × 256 pixels, 160 slices). Further imaging parameters were: Field of view (FOV) = 240 × 240 mm^2, echo-time TE = 3.8 ms, repetition-time TR = 8.27 ms, flip-angle α = 8°; sensitivity encoding (SENSE) factor R = 1.5. Total acquisition time was 8 min 23 s per scan.

A fast gradient echo echo-planar imaging sequence was applied in the functional part of the study in order to obtain BOLD scans at rest as well as during auditory stimulation. 300 functional volumes were acquired with a measured spatial resolution of 3.0 x 3.0 x 3.7 mm^3 (acquisition matrix 80 x 78 pixels, 35 slices) and a reconstructed spatial resolution of 3.0 x 3.0 x 3.7 mm^3 (reconstruction matrix 80 x 80 pixels, 35 slices). Further imaging parameters were: FOV = 240 x 240 mm^2; TE = 30.0 ms; TR = 1,960 ms; flip-angle $\alpha = 83°$; SENSE factor R = 2.2. Total acquisition time was about 13 minutes (7 minutes auditory control condition without auditory stimulation, 6 minutes auditory stimulation) and 5 minutes (resting state), respectively.

A T1-weighted fast field echo (FFE) sequence was used to map the B_0 field. The B_0 map (3D echo sequence) is composed of a magnitude and a phase image and was measured with a spatial resolution of 2.0 x 4.0 x 4.0 mm^3 (acquisition matrix 112 × 56 pixels, 75 slices). Further imaging parameters were: FOV = 224 × 224 x 120 mm, dual echo-time TE = 3.6/5.63 ms, repetition-time TR = 30.0 ms, flip-angle $\alpha = 60°$; total acquisition time was 4 min 11 s.

The B_1 field was also mapped using a T1-weighted FFE sequence. The B_1 map was calculated by the MRI scanner software using a dual repetition method, the actual flip angle method (AFI) (Yarnykh, 2007), with TR = 30.0/150 ms and flip-angle $\alpha = 60°$. Further imaging parameters were: FOV = 400 × 400 x 120 mm^3, echo-time TE = 2.2 ms, spatial resolution of 5.9 x 6.0 x 12.0 mm^3 (acquisition matrix 68 × 67 pixels, 20 slices); total acquisition time was 3 min 40 s.

2.3 Electroencephalographic system

MR images were recorded with and without the presence of a MR-compatible (field isolation containment) high-density EEG Geodesic Net Amp system with 256 channels (Electrical Geodesics, Eugene, Oregon). Electrode cables run down along the subjects back, leaving the

scanner parallel to the subjects' legs. Before EEG cap application, the sponge-equipped electrodes were soaked with salted water (potassium chloride) and shampoo, as done during usual EEG recordings, to achieve best possible electrical conductivity. The distribution of the electrodes on the scalp is depicted in Supplementary Figure 1.

2.4 Surface-based morphometry (SBM)

Differences in cortical morphological features such as cortical thickness, cortical surface area, and cortical volume between the conditions with and without the EEG cap were evaluated by using surface-based morphometry (SBM). Cortical surface reconstruction, cortical parcellation, as well as subcortical volumetric segmentation were performed with the FreeSurfer image analysis suite (version 5.3.0), one of the commonly used surface-based morphometric tools, which is documented and freely available online (http://surfer.nmr.mgh.harvard.edu). The technical details of these procedures are described in prior publications (Fischl et al., 1999a; Fischl et al., 2001; Fischl and Dale, 2000; Fischl et al., 2002; Fischl et al., 2004a; Fischl et al., 1999b; Fischl et al., 2004b). The 3D structural T1-weighted MRI scan was used to construct models of each subject's cortical surface in order to measure cortical thickness and cortical surface area. This fully automated procedure comprised segmentation of the cortical white matter (Fischl et al., 1999b), tessellation of the grey/white matter junction, inflation of the folded surface tessellation patterns (Fischl et al., 1999a; Fischl et al., 1999b) and an automatic correction of topological defects in the resulting manifold (Fischl et al., 2001). This surface was then used as starting point for a deformable surface algorithm designed to find the grey/white and pial (grey matter / cerebrospinal fluid (CSF)) surfaces with sub-millimetre precision (Fischl and Dale, 2000). The procedures for measuring cortical thickness have been validated against histological analysis (Rosas et al., 2002) and manual measurements (Kuperberg et al., 2003; Salat et al., 2004). This method uses both intensity and continuity information from the surfaces in the deformation procedure

in order to interpolate surface locations for regions in which the MRI image is ambiguous (Fischl and Dale, 2000). For each subject, cortical thickness of the cortical ribbon was computed on a uniform grid (comprised by vertices) with 1 mm spacing across both cortical hemispheres, with the thickness being defined by the shortest distance between the grey/white and pial surface models. Cortical area was estimated by computing the area of each vertex in a standardized, spherical atlas space surface tessellation and mapped back into the individual subject space. The calculation of cortical volume is a vertex-wise multiplication of cortical thickness and cortical area. The thickness and area maps produced are not limited to the voxel resolution of the image and thus sensitive for sub-millimetre differences between groups (Fischl and Dale, 2000). The way in which the resolution of the cortical maps goes beyond the resolution of the original acquisition is conceptually similar to a (conventional) partial volume correction procedure. The cortex is smooth at the spatial scale of several millimetres, which is imposed as constraint by FreeSurfer to estimate the location of the surface with subvoxel accuracy. For instance, if a given voxel is darker than its neighbouring grey matter it probably contains more CSF and so the surface model is at a slightly different position than if the neighbouring voxels were brighter and therefore contain probably more white matter. Cortical thickness, surface area, and volume measures were mapped to the inflated surface of each participant's brain reconstruction, this allowing visualization of data across the entire cortical surface (gyri and sulci) without the data being obscured by cortical folding. Data were re-sampled for all subjects and rendered onto a common spherical coordinate system (Fischl et al., 1999a). Then a surface-based vertex-wise cortical thickness, surface area, and volume map were computed for each participant. For the whole-brain vertex-wise analysis, the data were smoothed on the surface tessellation using an iterative nearest- neighbour averaging procedure with 148 iterations on the left hemisphere and 147 iterations on the right hemisphere, corresponding to a 2D surface-based diffusion smoothing kernel with a full with at half maximum (FWHM) of about 15 mm.

In addition, the cerebral cortex was parcellated into units based on gyral/sulcal structure as implemented in FreeSurfer (Desikan et al., 2006; Destrieux et al., 2010; Fischl et al., 2004b) and the subcortical brain structures were fully-automatically segmented into regions of interest (ROIs), of which the volumes were computed.

2.5 Voxel-based morphometry (VBM)

Differences in probabilistic grey matter volume between the cap and noncap condition were evaluated by using VBM (Ashburner and Friston, 2000; Good et al., 2001). All pre-processing steps were performed with the VBM8 toolbox (release 435, http://dbm.neuro.uni-jena.de/vbm/download/) that uses statistical parametric mapping (SPM8, release 4667, http://www.fil.ion.ucl.ac.uk/spm/) software. The following pre-processing steps were realized: (1) the coordinate origin of each native image was manually set on the anterior commissure. (2) Intensity inhomogeneity (bias field) correction, tissue class segmentation, and spatial normalization (affine and warping) were performed using unified segmentation (Ashburner and Friston, 2005) combined with SPM8's "new segmentation approach". For spatial normalization, the diffeomorphic anatomical registration using exponentiated lie algebra (DARTEL) approach was used (Ashburner, 2007). Canonical a priori maps (ICBM 452 T1-weighted) implemented in SPM8 were used as reference templates. (3) To enhance tissue class segmentation, Hidden Markov Random Field (HMRF) modulation was applied (http://dbm.neuro.uni-jena.de/vbm/markov-random-fields/) (Cuadra et al., 2005). (4) To investigate absolute volumes, the warped images were voxel-wise multiplied with the Jacobian determinant of the deformations (linear as well as nonlinear terms were modulated). (5) The resulting Jacobian and HMRF modulated and segmented GM images were smoothed with a Gaussian kernel of FWHM = 9 mm and the additional smoothing introduced during the modulation process was about FWHM = 3 mm.

2.6 Preprocessing of resting state fMRI data

Functional MRI data were preprocessed with DPARSF toolbox (version 2.0) (Chao-Gan and Yu-Feng, 2010) using functions of SPM 8 (www.fil.ion.ucl.ac.uk/spm/software/spm8). The following steps were realised: 1) slice timing correction, 2) realignment, 3) linear and non-linear normalization onto a standard EPI template, 4) voxel re-sampling to 2 x 2 x 2 mm^3, 5) smoothing with a Gaussian kernel of 8 mm full width at half maximum, 6) detrending, 7) filtering (such that frequencies $0.01 < f < 0.08$ Hz passed the filter), 8) regressing out the variance of nine nuisance covariates: six parameters from head motion correction (three translation, three rotation parameters) as well as the global mean signal, white matter signal and cerebrospinal fluid signal based on standard masks implemented in SPM 8. Local maxima MNI coordinates for the precuneus / posterior cingulate cortex (classical seed region for the default mode network) were obtained from a study published by Greicius and colleagues (Greicius et al., 2003). Next, 5-mm radius spherical ROIs were created centred on the respective coordinates (MNI; 5, -51, 27 for right precuneus and -5, -51, 27 for left precuneus) using Wake Forest University Pickatlas toolbox (Maldjian et al., 2003). We used combined seed ROIs incorporating both right and left hemispheric parts of the precuneus. For both seed ROIs, mean signal time course was computed and used as regressor in a voxel-wise resting state functional connectivity (rsFC) analysis using functions of REST toolbox 1.6 (Song et al., 2011). For each subject and each seed ROI, one whole-brain correlation map was obtained (first-level). Next, each map was *r*-to-*z*-transformed to yield normal distribution for parametric group analysis (second-level).

2.7 Preprocessing of auditory task-related fMRI data

To find any putative influences of the anatomical image with and without the EEG cap on fMRI preprocessing, a session of auditory stimulation (block of six minutes) was contrasted

against resting state (eyes open, block of seven minutes). A standard preprocessing procedure was applied on the functional data. Images were realigned and unwarped (B_0 map was calculated from the functional data) using field map to correct for motion and susceptibility artefacts and motion-by-susceptibility interactions (Andersson et al., 2001; Hutton et al., 2002). To investigate a putative bias of the EEG cap on the spatial normalization procedure of the functional data time series, in two different analyses, the individual T1-weighted images recorded with and without the EEG cap were transformed separately on a T1-template in MNI space, using the unified segmentation approach by Ashburner and Friston (Ashburner and Friston, 2005). The data were spatially smoothed with a FWHM of a 8mm Gaussian kernel. First level analysis on the individual level was performed using a general linear model. The design matrix included two conditions, namely an auditory control condition (resting state with eyes open) and an auditory stimulation. Furthermore, the standard hemodynamic response function as well as a standard high-pass filter (128s cut-off) was applied. To test for statistical significant voxels, a second-level analysis was calculated with t-statistics against zero for within group effect. Afterwards, the resulting statistical parametric maps of fMRI analyses including the anatomical image either with or without the cap in the spatial normalization step across subjects were overlaid and visually inspected and compared. In addition, a mean image was created for the T1-weighetd images of all subjects with the EEG cap and a mean image for all anatomical images without the cap and overlaid to visualize anatomical differences between the T1-weighted image with and without the EEG cap (see Figure 4).

2.8 Computation of the SNR

The spatial white matter SNR of the T1-weighted images was computed by FreeSurfer's quality assessment (QA) tools (http://ftp.nmr.mgh.harvard.edu/fswiki/QATools) using the

"wm-anat-snr" function. Voxels that has been labelled by FreeSurfer automatic segmentation procedure (see aparc+aseg.mgz file) as cerebral, cerebellar, and callosal white matter as well as voxels labelled as white matter hypointensities were considered for spatial SNR computation. With this tool, the spatial SNR has then been computed by dividing the mean intensity value of all voxels within the above-mentioned labels by the SD of these white matter voxels. The spatial gray matter SNR values were provided by the common FreeSurfer processing stream (as described in 2.4) from the "lh/rh.w-g.pct.stats" and the "aseg.stats" file. As described for calculation of the white matter SNR, voxels that has been labelled by FreeSurfer automatic segmentation procedure (see aparc.mgz file) as cerebral and cerebellar gray matter entered spatial gray matter SNR computation by dividing the mean of the gray matter signals by the SD of these signals.

The temporal SNR was calculated in Matlab with the sd_images.m script (http://dbic.dartmouth.edu/wiki/index.php/Noise_Detection) by dividing voxel-wisely (across the whole head) the mean of the signal by the SD of these voxels across all time series.

2.9 Preprocessing of B_0 field map

The following preprocessing steps were applied to the B_0 field map: 1) The magnitude images of both the cap and noncap condition, which are in the same space as the corresponding B_0 maps, were spatially normalised onto the T1-weighted template delivered with the SPM software using both linear and nonlinear transformations. 2) These transformations were applied to the B_0 map of the cap and noncap condition, respectively. 3) The B_0 maps were then smoothed using a Gaussian kernel of FWHM = 8 mm. Effect size was calculated based on Cohen's d using pooled variance of the local minimum or maximum of the cluster with the lowest and that with the highest p-value.

2.10 Preprocessing of B_1 field map

The following preprocessing steps were applied to the B_1 field map: 1) One of the magnitude images of the noncap condition, which is in the same space as the corresponding B_1 map, was co-registered to the subjects T1-weighted image derived from the noncap condition and these transformations were applied to the noncap B_1 map. 2) One of the magnitude images in the cap condition, which is also in the same space as the corresponding B_1 map, was co-registered to the co-registered magnitude image from the noncap condition (step 1) and these transformations were applied to the cap B_1 map. 3) The T1-weighted image was spatially normalised onto the T1-weighted template delivered with the SPM software using both linear and nonlinear transformations and these transformations were applied to both co-registered B_1 maps. 4) The B_1 maps were then smoothed using a Gaussian kernel of FWHM = 8 mm. Effect size was calculated based on Cohen's d using pooled variance of the local minimum or maximum of the cluster with the lowest and that with the highest p-value.

2.11 Individual B_0 and B_1 analysis

In order to investigate individual differences of the B_0 and B_1 field maps dependent on if the subject wore the EEG cap in the scanner or not, we computed voxel-wisely a mean and a SD map (whole head) across all subjects of the B_0 and B_1 field map in the noncap and the cap condition, respectively. Afterwards, the individual B_0 and B_1 field maps of the cap condition were z-transformed using the mean and SD of the noncap condition, reflecting the cap > noncap contrast of the group analysis. The individual B_0 and B_1 field maps of the noncap condition were analyzed accordingly and z-transformed using the mean and SD of the cap condition, representing the noncap > cap contrast of the group analysis.

2.12 Statistical analyses

For all imaging data, vertex- or voxel-wise general linear models (GLM) for repeated measures were applied using either parametric testing (SBM, resting state fMRI, B_0 and B_1 map) or permutation-based non-parametric testing (VBM) that also corrects for multiple comparisons across space. For VBM data, the threshold free cluster enhancement (TFCE) technique was used in addition (Smith and Nichols, 2009).

For the SBM data, a GLM based on parametric statistics was applied within FreeSurfer software (mri_glmfit tool) without using TFCE. Error probability was set at $p < 0.05$ combined with a false discovery rate (FDR) correction (see Figure 1, Supplementary Figure 2 and 3). For the VBM data, a GLM based on non-parametric statistics was applied within FSL software (randomise tool) using TFCE. Error probability was set at $p < 0.05$ combined with permutation-based corrections for multiple comparisons across space (see Supplementary Figure 4).

For the B_0 and B_1 field maps, GLMs based on parametric statistics was applied within SPM software (paired *t* test) without using TFCE (see Figure 3). Here, we did not apply any correction for multiple comparisons for several reasons. The sample size was rather small ($n = 5$), the B_0 and B_1 field maps showed differential effect sensitivity, and also in order to decrease the beta error probability, i.e. the probability to miss an effect that is real.

For the resting state fMRI data, a voxel-wise one-sample *t* test examining whether the correlation coefficient (*z*-value) was different from zero, indicating positive resting state functional connectivity (rsFC) was applied within the SPM software (see Figure 2). Furthermore, a paired *t* test was computed between the two conditions (with versus without the EEG cap) to test for putative significant effect of the EEG cap on rsFC. In order to find significant voxels in auditory stimulation condition, an one-sample *t* test against zero was performed. This *t* test was performed twice, once for the preprocessed data including the individual T1-weighted image with the EEG cap in the spatial normalisation step and once for the control condition, i.e. the data with the individual anatomical image without the EEG cap

included in the normalization step. For visualization, we have then overlayed the respective statistical parametric maps of the cap and the noncap condition (see Figure 4A).

For the comparisons of global brain measures, volumes of subcortical structures, and the SNR of the T1-weighted images, IBM SPSS statistics 20 was used (SPSS, an IBM company, Armonk, New York) without any correction for multiple comparisons.

3. Results

The measurement of cortical thickness with the T1-weighted MR data show an increased cortical thickness of approximately 0.14 mm in frontal regions of the left and 0.17 mm of the right hemisphere and a strong decrease over the temporal lobe of -0.25 mm in the left and -0.29 mm in the right hemisphere (paired *t* test, FDR = 0.05), when subjects wear the EEG cap in the scanner (see Fig. 1). These values are in the range of around 10% of the averaged cortical thickness in humans (Han et al., 2006; Sowell, 2004). The influence of the EEG cap also yields a negative effect on volumetric measurements of subcortical structures (see Supplementary Table 1-3) as well as on cortical volume and surface area measurements (data shown in Supplementary Fig. 2 and 3). Analysis of the voxel-based morphometry delivered comparable results (see Supplementary Figure 4). A consistent influence of the EEG cap on cortical thickness of every single subject that entered the group level surface-based analysis is depicted in Supplementary Figure 5.

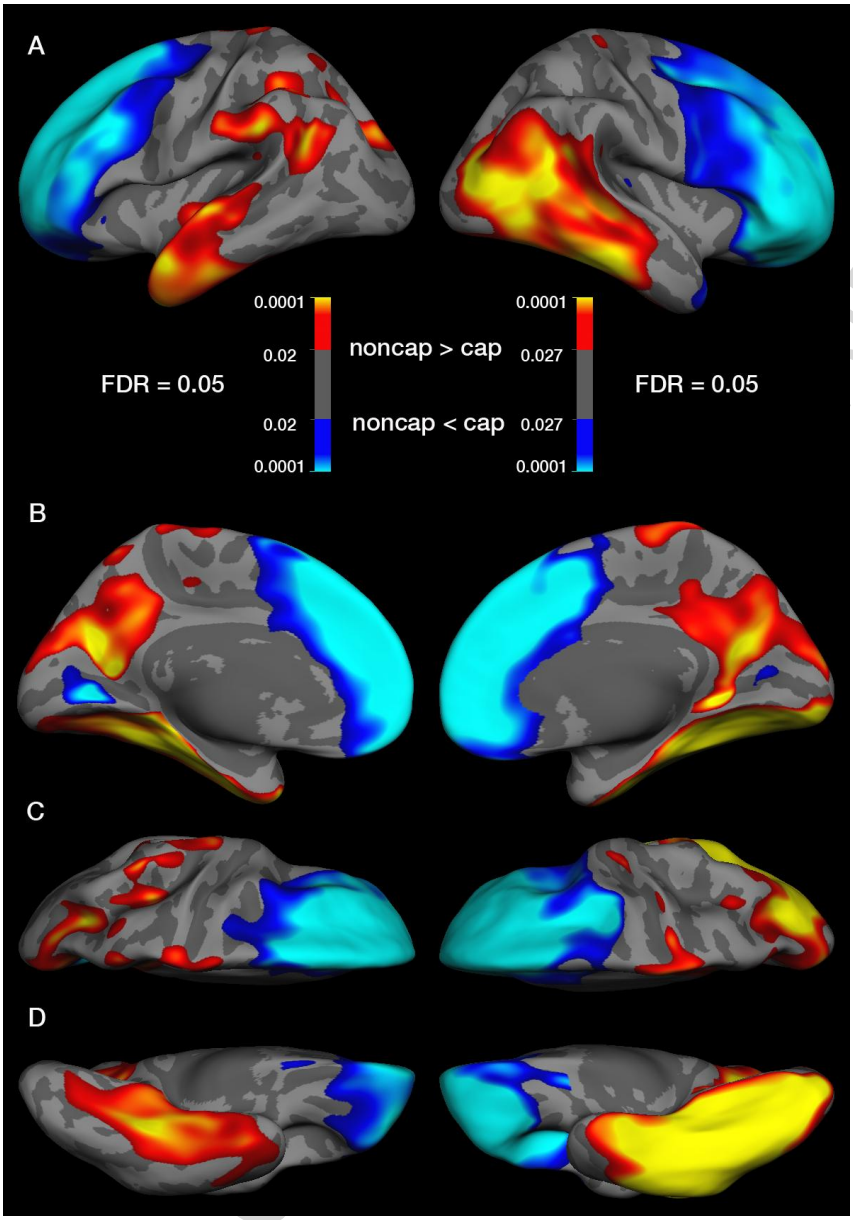

Figure 1. The influence of the high-density EEG net on cortical thickness measurement derived from surface-based morphometry of T1-weighted images shown on lateral (A), medial (B), superior (C), and inferior (D) view of the left (left column) and right (right column) hemisphere. Cortical thickness is increased over frontal cortical areas (blue) and significantly decreased over the temporal lobe (yellow-red) when subjects do wear the EEG cap (paired *t* test, FDR = 0.05 false discovery rate corrected). The colour bar represents FDR-corrected p-values.

In contrast to the findings reported by Luo and Glover (Luo and Glover, 2012), the evaluation of the SNR for both the structural (spatial SNR) and functional (temporal SNR) images revealed a significantly consistently higher value for the measurements when subjects did not wear an EEG cap compared to when wearing the net (T1-weighted images: mean spatial SNR of white matter without cap: 24.3, SD 1.49; mean spatial SNR of white matter with EEG cap: 20.3, SD 1.73; paired *t* test, $T_{12} = 6.079$, $p < 0.001$ uncorrected; mean spatial SNR of gray matter without cap: 4.23, SD 0.14; mean spatial SNR of gray matter with EEG cap: 4.04, SD 0.14; paired *t* test, $T_{12} = 8.134$, $p < 0.001$ uncorrected; T2*-weighted images: mean temporal SNR without cap: 77.46, SD 14.18; mean temporal SNR with EEG cap: 70.92, SD 13.69; paired *t* test, $T_4 = 2.974$, $p < 0.005$ uncorrected).

Results of the seed-based analysis of resting state activity with respect to the precuneus (MNI; 5, -51, 27 for right precuneus and -5, -51, 27 for left precuneus) as part of the default-mode network (DMN) are depicted in Figure 2 (one-sample *t* test against zero, $T_9 = 4.29$, $p < 0.001$ for the cap as well as the non-cap condition, uncorrected). Correlations are comparable with and without the EEG cap and hemodynamic activity was found at typical DMN locations, such as the precuneus/retrosplenial cortex, the anterior cingulate cortex, the posterior cingulate cortex, and the medial prefrontal regions (Raichle et al., 2001). A paired *t* test between the two conditions did not reveal a significant difference in terms of hemodynamic fluctuations.

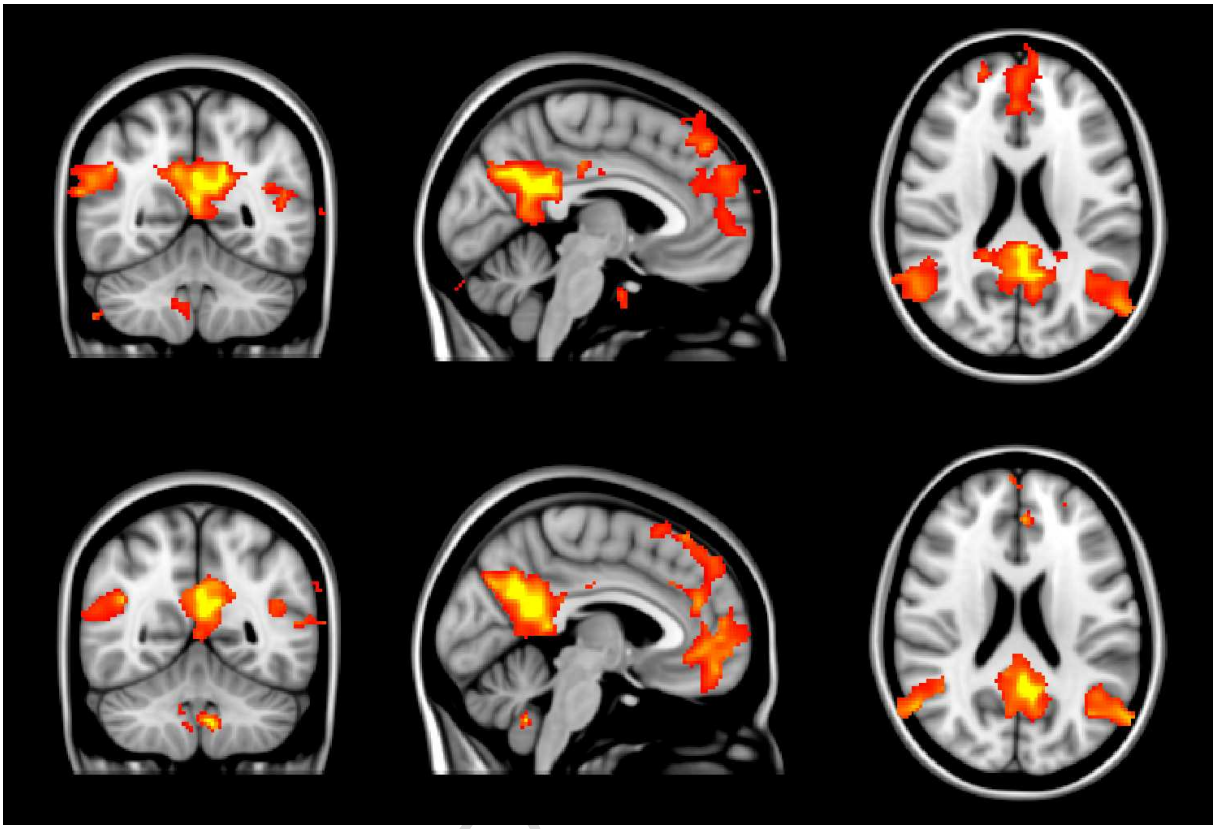

Figure 2. Correlations of the resting state activity with the precuneus seed hemodynamic fluctuation for the DMN with the EEG cap (upper row) and without the cap (lower row; one-sample *t* test against zero, $T_9 = 4.29$, $p < 0.001$ uncorrected, k = 20 voxels for the cap as well as the non-cap condition).

As shown in Figure 3, analysis of B_0 and B_1 maps revealed significant local perturbations of the field maps over frontal, fronto-temporal and parietal regions with and without the EEG net, respectively, with a stronger perturbation of the B_1 map over the right compared to the left hemisphere (B_0: paired *t* test, $T_4 = 2.13$, $p < 0.05$ uncorrected, effect size according Cohen's d ≥ 0.735 for the noncap > cap contrast and d ≥ 0.783 for the cap > noncap contrast; B_1: paired *t* test, $T_4 = 7.17$, $p < 0.001$ uncorrected, effect size according Cohen's d ≥ 3.404 for the noncap > cap contrast and d ≥ 3.095 for the cap > noncap contrast). Raw data of B_1 field map inhomogeneities on the example of a single subject are shown in Supplementary Figure 6. In Supplementary Figure 7 and 8, z-transformed B_0 and B_1 field maps are depicted on the single-subject level.

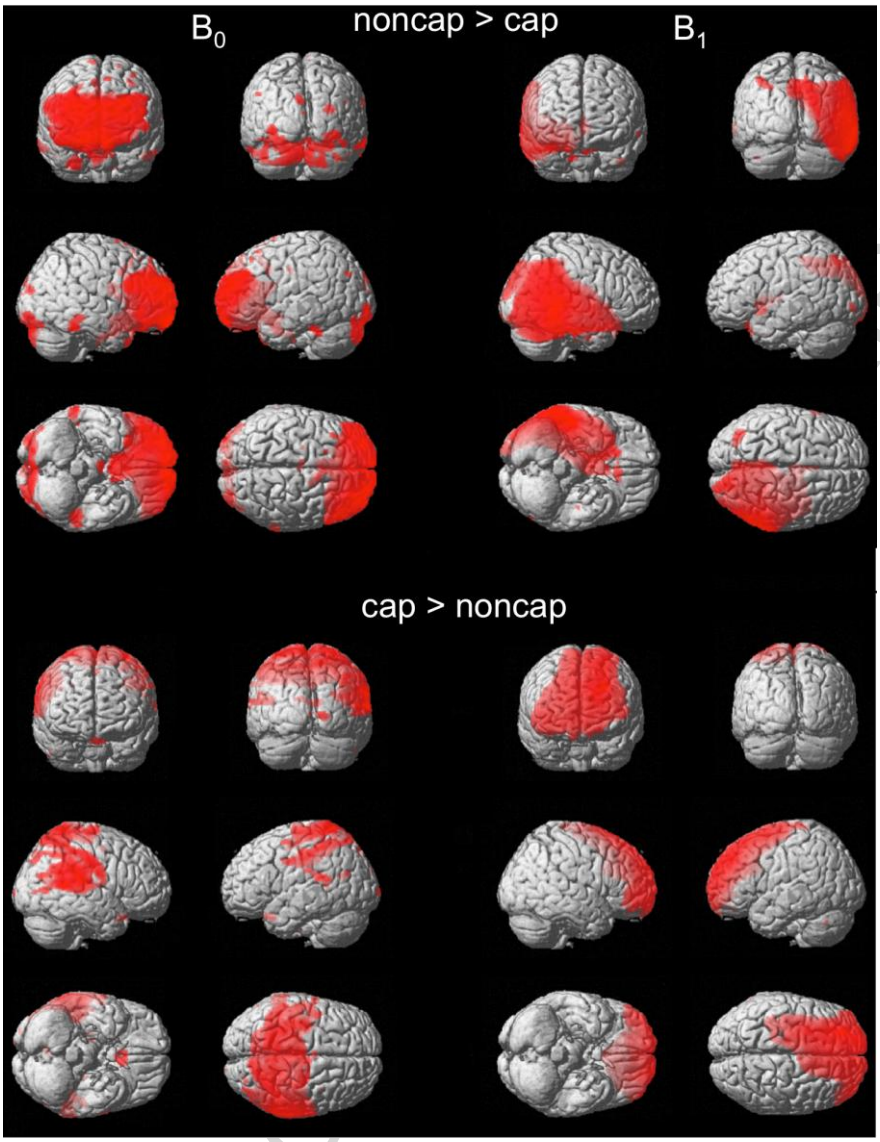

Figure 3. Statistical differences of B_0 (left column) and B_1 (right column) field map inhomogeneities for both contrasts noncap > cap and cap > noncap (B_0: paired *t* test, T_4 = 2.13, $p < 0.05$ uncorrected, effect size according Cohen's $d \geq 0.735$ for the noncap > cap contrast and $d \geq 0.783$ for the cap > noncap contrast; B_1: paired *t* test, $T_4 = 7.17$, $p < 0.001$ uncorrected, effect size according Cohen's $d \geq 3.404$ for the noncap > cap contrast and $d \geq 3.095$ for the cap > noncap contrast). Local field inhomogeneities are present over the frontal, parietal, and temporal lobe with an emphasis on the right hemisphere for left-right asymmetry.

To understand putative differences in the analysis of the functional data due to anatomical differences caused by the EEG cap, T1-weighted images one with and one without the EEG cap were included separately in the spatial normalization step of fMRI preprocessing (one-sample *t* test against zero, $T_5 = 2.015$, $p < 0.05$ uncorrected; see Fig. 4 A). The activations in response to the auditory stimulation occur nearly in the same brain regions on the statistical parametric maps, with the activation slightly shifted upwards in z-direction when including the anatomical image with the EEG cap. Therefore, functional MRI seems to deliver reliable results, independent of including the individual T1-weighted image without or even with the EEG cap. Figure 4 B-D indicates in which brain regions the T1 images (average across group) with and without the EEG cap differ in size and shape. Therefore, with help of the "slices" function in the FSL software, we overlaid the averaged T1 images across all participants without the EEG cap with the averaged T1 images when subjects wore the EEG cap (background image). Some slight edge effects at, for example, the corpus callosum and the outermost borders of the grey matter of the cortex are visible.

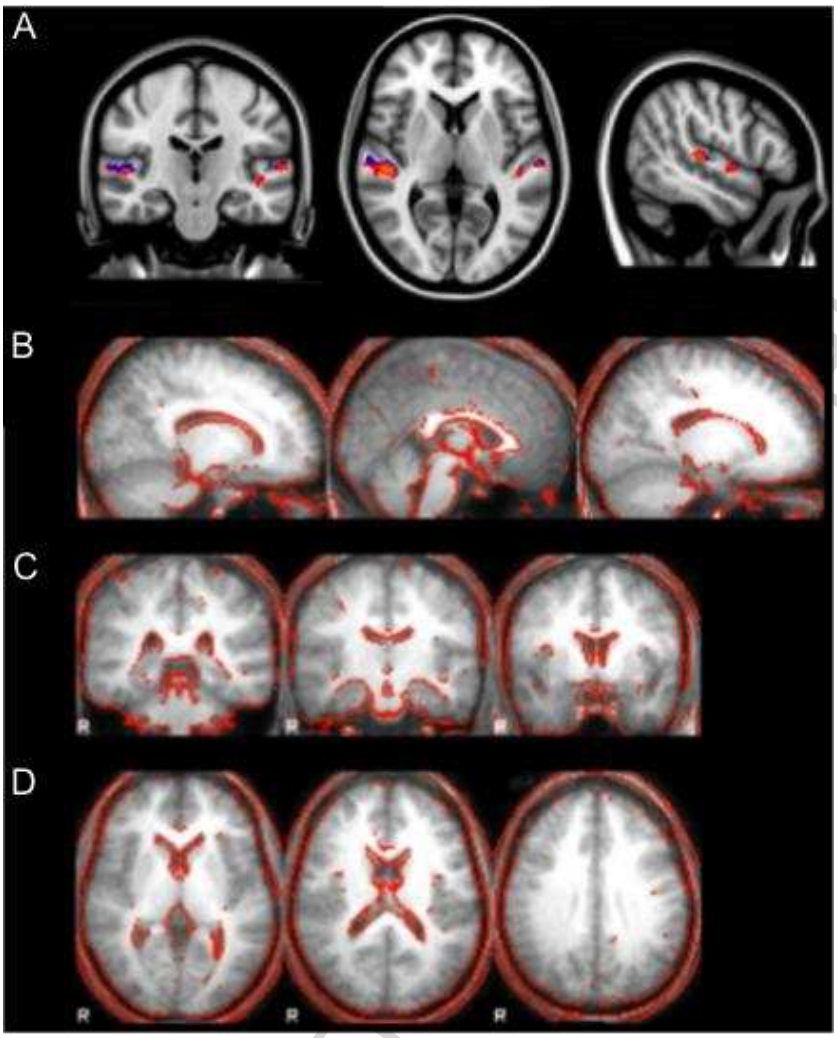

Figure 4. (A) Overlay of the statistical parametric maps of the functional data during listening to music versus resting state activity, once using the T1-weighted image with the high-density EEG cap (blue) and once without (yellow-red) during spatial normalisation on a T1-weighted template (one-sample *t* test against zero, $T_5 = 2.015$, $p < 0.05$ uncorrected). (B-C) Overlay of brain slices of averaged T1-weighted images of all subjects with (background image) and without the EEG cap of (B) sagittal, (C) coronal, and (D) horizontal orientations. The red line indicates in which regions the T1-weighted image without the EEG cap differs in shape compared to the T1-weighted image with the EEG cap (background image).

4. Discussion

In order to extend the current knowledge about the influence of a high-density EEG cap on MRI data quality, we recorded T1- and T2*-weighted images as well as B_0 and B_1 field maps of subjects during both a simultaneous EEG-MRI measurement as well as with MRI only. To this end, we analyzed both the functional and anatomical data in conventional ways often used in the neuroscientific community (see Methods).

Analysis of the SNR showed a consistent reduction for both the functional and structural data, which is in line with previous studies (Mullinger et al., 2008; Vasios et al., 2006). Therefore, we conclude that with a reduced SNR, weaker brain activation might get overlooked in simultaneous EEG-fMRI recordings in contrast to sole fMRI data acquisitions and thus, important findings might get disregarded by conservatively correcting the p-value.

Regarding the T1-weighted images, we observed a strong effect of the EEG cap on structural morphometric measurements, in particular over the frontal and temporal lobes, which was more pronounced on the right hemisphere (see Figure 1). The observed effect amounted to approximately 10% of the average cortical thickness in humans (Han et al., 2006; Sowell, 2004), reflecting a strong decrease in data quality. By comparing the results of cortical volume morphometric measure, which is a simple vertex-wise multiplication of cortical thickness and surface area, it becomes obvious, that the EEG cap leads to an increased vertical orientation (i.e. cortical thickness, Fig. 1) of disturbance of the MR signal rather than a horizontal one (i.e. surface area, Suppl. Fig. 2). This, in turn, explains the increased influence of the cortical thickness on the volume measures (Suppl. Fig. 3) compared to the area measures.

In addition to the anatomical images, inhomogeneities of the B_0 and B_1 field maps were observed, showing that the EEG cap has a negative impact on both the static magnetic field as

well as the radio frequency (RF) pulse, as has been reported in a previous study by Mullinger and colleagues (Mullinger et al., 2008). Comparing the affected brain regions of the T1-weighted images with perturbations of the B_0 and B_1 field maps (see Figure 3), regional consistencies arise. In this context, inhomogeneities in the gradient field seem to lead to a decreased cortical thickness over the temporal lobe, whereas the increase in cortical thickness of frontal regions caused by the EEG cap seem to be ascribed to the frontal disruptions of both the B_0 and the B_1 field map. Thus, the interplay between the affected static magnetic field and the RF pulse seems to affect the anatomical image. A possible explanation for this finding might be that high frequencies such as the RF pulse (128MHz at 3T) induce currents in the electrodes and/or electrode wires. Thereby, the resulting electro-magnetic fields interact with the B_1 field, leading thus to local changes of signal intensities. On the other hand, the electrically conductive material in the EEG cap as well as eddy currents in the electrodes induced by the gradient field might also cause perturbation of the static magnetic field B_0. In the previous study by Mullinger and colleagues (Mullinger et al., 2008), frontal and parietal perturbations of the B_0 field maps appeared to be risen by ECG and EOG leads in contrast to inhomogeneities in the B_1 maps resulting from single electrodes that increase in severity with field strength. This finding cannot be supported by our results since the EEG system used in the present study does not include extra EOG and ECG leads passing the subjects' heads. Moreover, the electrodes of the EEG cap are evenly distributed over the head (see Supplementary Figure 1), not showing any left-right asymmetric arrangement of the conductive parts (electrodes/electrode wires). Consequently, the asymmetric intensity distribution of the B_0 field map induced by the gradient field is not caused by the spatial arrangement of the electrically conductive material of the EEG cap. A more plausible explanation might be the fact that the RF field is rotating (around the main magnetic field axis), which results in a left-right asymmetric alteration of the B_0 field homogenities. Changes in the B_0 field might ultimately lead to a distorted allocation of brain tissue to the voxels

during data acquisition, in particular at the borders between different tissues. As depicted in Figure 4B, the inaccurate assignment of voxels to brain tissue types cannot be corrected by applying standard normalization processing. In order to exactly explain or to find a way to reduce or compensate the anterior-posterior and left-right asymmetry of the signal intensities of the B_1 and B_0 maps, information about the local differences in the electromagnetic field distributions are needed, which would require a full electromagnetic field simulation of the RF shield, the RF coil as well as a head model with and without the EEG cap. This is out of scope for this publication (for first steps of B_1 and B_0 map improvement, see (Katscher and Bornert, 2006; Schneider et al., 2013)). In this context, another aspect worth to be mentioned is a putative influence of changes of the impedance of the electrodes during measurement, which might affect data quality of the MRI images. Due to ventilation in the scanner, frontal electrodes are expected to dry out first, leading to an increased impedance and thus to a worse signal quality of the EEG. Whether such changes of impedance values might lead to changes in MR signal quality was not tested here and remains an open question.

A comparison of the T2*-weighted images did not reveal the EEG cap having an impact on the localization of brain activity for either the seed-based analysis of the resting state data or on the involvement of the individual T1-weighted images with and without the EEG cap in the spatial normalization step of the fMRI preprocessing. Thus, in contrast to the anatomical data, the worse spatial resolution of the functional images ($3x3x3mm^3$) leads to a decreased sensitivity of an inaccurate assignment of brain tissue to the respective voxel.

5. Conclusion

In summary, our findings reveal a strong sequence-dependent influence of high-density EEG caps on MRI data quality. Our results report a decreased SNR for both the anatomical and functional sequence during a simultaneous recording of EEG and MRI, as well as reliable results for the localization of brain activity for the functional data, but also a strong influence

of the EEG cap on morphometric measurements. Based on these facts, we strongly advice against the measurement of T1-weighted images simultaneously with high-density EEG caps, despite the benefit on time and as long as no final solution has been found for correcting the artefacts caused by the EEG setup. Even though this study provides new insights on the interaction of high-density EEG caps and MRI data, we want to emphasize that our findings are restricted to the field strength and particular EEG setup used in this work. However, as suggested by Mullinger and colleagues (Mullinger et al., 2008), a decreased destruction of anatomical images might be expected with fewer electrodes and reduced field strength. To draw any final conclusions regarding this issue, further studies are needed.

Acknowledgment

This project was funded by the SNF (Swiss National Science Foundation) Sinergia-Grant #136249 to LJ. Part of the data discussed in this paper have been presented at the International Conference on Basic an Multimodal Imaging (BaCI) in Geneva, Switzerland, 2013 (Klein et al., 2013).

Author contributions

CK designed the study, recorded the data, and analysed the data together with JH. JH supervised data analysis. CK and JH wrote the paper. RL helped with physical background of result interpretation. LJ supervised research and contributed to the manuscript. All authors have read and approved the final version of the manuscript.

Competing financial interests

The authors declare no competing financial interests.

References

Andersson, J. L., Hutton, C., Ashburner, J., Turner, R., and Friston, K. (2001). Modeling geometric deformations in EPI time series. *NeuroImage, 13*(5), 903-919. doi: 10.1006/nimg.2001.0746

Ashburner, J. (2007). A fast diffeomorphic image registration algorithm. *NeuroImage, 38*(1), 95-113. doi: 10.1016/j.neuroimage.2007.07.007

Ashburner, John, and Friston, Karl J. (2000). Voxel-Based Morphometry--The Methods. *NeuroImage, 11*(6), 805-821.

Ashburner, John, and Friston, Karl J. (2005). Unified segmentation. *NeuroImage, 26*(3), 839-851.

Bonmassar, G.; Hadjikhani, N.; Ives, J.R.; Hinton, D.; Belliveau, J.W. (2001). Influence of EEG electrodes on the BOLD fMRI signal. *Hum Brain Mapp, 14*(2), 108-115.

Chao-Gan, Y., and Yu-Feng, Z. (2010). DPARSF: A MATLAB Toolbox for "Pipeline" Data Analysis of Resting-State fMRI. *Front Syst Neurosci, 4*, 13. doi: 10.3389/fnsys.2010.00013

Cuadra, M. B., Cammoun, L., Butz, T., Cuisenaire, O. A. , and Thiran, J. P. A. . (2005). Comparison and validation of tissue modelization and statistical classification methods in T1-weighted MR brain images. *IEEE Trans Med Imaging, 24*(12), 1548-1565.

Desikan, Rahul S., Ségonne, Florent, Fischl, Bruce, Quinn, Brian T., Dickerson, Bradford C., Blacker, Deborah, Buckner, Randy L., Dale, Anders M., Maguire, R. Paul, Hyman, Bradley T., Albert, Marilyn S., and Killiany, Ronald J. (2006). An automated labeling system for subdividing the human cerebral cortex on MRI scans into gyral based regions of interest. *NeuroImage, 31*(3), 968-980.

Destrieux, Christophe, Fischl, Bruce, Dale, Anders, and Halgren, Eric. (2010). Automatic parcellation of human cortical gyri and sulci using standard anatomical nomenclature. *NeuroImage, 53*(1), 1-15.

Fischl, B, Sereno, M. I. , Tootell, R. B. H. , and Dale, A. M. (1999a). High-resolution intersubject averaging and a coordinate system for the cortical surface. *Hum Brain Mapp, 8*(4), 272-284.

Fischl, B., Liu, A., and Dale, A. M. (2001). Automated manifold surgery: constructing geometrically accurate and topologically correct models of the human cerebral cortex. *IEEE Trans Med Imaging, 20*(1), 70-80.

Fischl, Bruce, and Dale, Anders M. (2000). Measuring the thickness of the human cerebral cortex from magnetic resonance images. *Proc Natl Acad Sci U S A, 97*(20), 11050-11055.

Fischl, Bruce, Salat, David H., Busa, Evelina, Albert, Marilyn, Dieterich, Megan, Haselgrove, Christian, van der Kouwe, Andre, Killiany, Ron, Kennedy, David, Klaveness, Shuna, Montillo, Albert, Makris, Nikos, Rosen, Bruce, and Dale, Anders M. (2002). Whole Brain Segmentation: Automated Labeling of Neuroanatomical Structures in the Human Brain. *Neuron, 33*(3), 341-355.

Fischl, Bruce, Salat, David H., van der Kouwe, Andre J. W., Makris, Nikos, Ségonne, Florent, Quinn, Brian T., and Dale, Anders M. (2004a). Sequence-independent segmentation of magnetic resonance images. *NeuroImage, 23*(Supplement 1), S69-S84.

Fischl, Bruce, Sereno, Martin I., and Dale, Anders M. (1999b). Cortical Surface-Based Analysis: II: Inflation, Flattening, and a Surface-Based Coordinate System. *NeuroImage, 9*(2), 195-207.

Fischl, Bruce, van der Kouwe, Andre, Destrieux, Christophe, Halgren, Eric, Ségonne, Florent, Salat, David H., Busa, Evelina, Seidman, Larry J., Goldstein, Jill, Kennedy, David, Caviness, Verne, Makris, Nikos, Rosen, Bruce, and Dale, Anders M. (2004b). Automatically Parcellating the Human Cerebral Cortex. *Cereb Cortex, 14*(1), 11-22. doi: 10.1093/cercor/bhg087

Good, Catriona D., Johnsrude, Ingrid S., Ashburner, John, Henson, Richard N. A., Friston, Karl J., and Frackowiak, Richard S. J. (2001). A Voxel-Based Morphometric Study of Ageing in 465 Normal Adult Human Brains. *NeuroImage, 14*(1), 21-36.

Greicius, M. D., Krasnow, B., Reiss, A. L., and Menon, V. (2003). Functional connectivity in the resting brain: a network analysis of the default mode hypothesis. *Proc Natl Acad Sci U S A, 100*(1), 253-258. doi: 10.1073/pnas.0135058100

Han, X., Jovicich, J., Salat, D., van der Kouwe, A., Quinn, B., Czanner, S., Busa, E., Pacheco, J., Albert, M., Killiany, R., Maguire, P., Rosas, D., Makris, N., Dale, A., Dickerson, B.,

and Fischl, B. (2006). Reliability of MRI-derived measurements of human cerebral cortical thickness: the effects of field strength, scanner upgrade and manufacturer. *NeuroImage, 32*(1), 180-194. doi: 10.1016/j.neuroimage.2006.02.051

Herrmann, C. S., and Debener, S. (2008). Simultaneous recording of EEG and BOLD responses: a historical perspective. *Int J Psychophysiol, 67*(3), 161-168. doi: 10.1016/j.ijpsycho.2007.06.006

Hutton, C., Bork, A., Josephs, O., Deichmann, R., Ashburner, J., and Turner, R. (2002). Image distortion correction in fMRI: A quantitative evaluation. *NeuroImage, 16*(1), 217-240. doi: 10.1006/nimg.2001.1054

Katscher, U., and Bornert, P. (2006). Parallel RF transmission in MRI. *NMR Biomed, 19*(3), 393-400. doi: 10.1002/nbm.1049

Klein, C., Hänggi, J., and Jäncke, L. (2013). The Influence of a High-Density EEG Cap on T1- and T2*-Weighted MR Images (Abstracts of Presentations at the International Conference on Basic and Clinical Multimodal Imaging (BaCI), a Joint Conference of the International Society for Neuroimaging in Psychiatry (ISNIP), the International Society for Functional Source Imaging (ISFSI), the International Society for Bioelectromagnetism (ISBEM), the International Society for Brain Electromagnetic Topography (ISBET), and the EEG and Clinical Neuroscience Society (ECNS), in Geneva, Switzerland, September 5-8, 2013). *Clin EEG Neurosci, 44*(4), E1-E121. doi: 10.1177/1550059413507209

Kuperberg, Gina R., Broome, Matthew R., McGuire, Philip K., David, Anthony S., Eddy, Marianna, Ozawa, Fujiro, Goff, Donald, West, W. Caroline, Williams, Steven C. R., van der Kouwe, Andre J. W., Salat, David H., Dale, Anders M., and Fischl, Bruce. (2003). Regionally Localized Thinning of the Cerebral Cortex in Schizophrenia. *Arch Gen Psychiatry, 60*(9), 878-888. doi: 10.1001/archpsyc.60.9.878

Luo, Q., and Glover, G. H. (2012). Influence of dense-array EEG cap on fMRI signal. *Magn Reson Med, 68*(3), 807-815. doi: 10.1002/mrm.23299

Maldjian, J. A., Laurienti, P. J., Kraft, R. A., and Burdette, J. H. (2003). An automated method for neuroanatomic and cytoarchitectonic atlas-based interrogation of fMRI data sets. *NeuroImage, 19*(3), 1233-1239. doi: S1053811903001691 [pii]

Michel, C. M., Murray, M. M., Lantz, G., Gonzalez, S., Spinelli, L., and Grave de Peralta, R. (2004). EEG source imaging. *Clin Neurophysiol, 115*(10), 2195-2222. doi: 10.1016/j.clinph.2004.06.001

Mullinger, K., Debener, S., Coxon, R., and Bowtell, R. (2008). Effects of simultaneous EEG recording on MRI data quality at 1.5, 3 and 7 tesla. *Int J Psychophysiol, 67*(3), 178-188. doi: 10.1016/j.ijpsycho.2007.06.008

Raichle, M.E., MacLeod, A.M., Snyder, A. Z., Powers, W.J., Gusnard, D.A, and Shulman, G. L. (2001). A default mode of brain function. *PNAS, 98*(2), 676-682.

Ritter, P., and Villringer, A. (2006). Simultaneous EEG-fMRI. *Neurosci Biobehav Rev, 30*(6), 823-838. doi: 10.1016/j.neubiorev.2006.06.008

Rosas, H. D., Liu, A. K., Hersch, S., Glessner, M., Ferrante, R. J., Salat, D. H., van der Kouwe, A., Jenkins, B. G., Dale, A. M., and Fischl, B. (2002). Regional and progressive thinning of the cortical ribbon in Huntington's disease. *Neurology, 58*(5), 695-701.

Salat, David H., Buckner, Randy L., Snyder, Abraham Z., Greve, Douglas N., Desikan, Rahul S. R., Busa, Evelina, Morris, John C., Dale, Anders M., and Fischl, Bruce. (2004). Thinning of the Cerebral Cortex in Aging. *Cereb. Cortex, 14*(7), 721-730. doi: 10.1093/cercor/bhh032

Schneider, R., Ritter, D., Haueisen, J., and Pfeuffer, J. (2013). B0-informed variable density trajectory design for enhanced correction of off-resonance effects in parallel transmission. *Magn Reson Med*. doi: 10.1002/mrm.24780

Smith, S. M., and Nichols, T. E. (2009). Threshold-free cluster enhancement: addressing problems of smoothing, threshold dependence and localisation in cluster inference. *NeuroImage, 44*(1), 83-98. doi: 10.1016/j.neuroimage.2008.03.061

Song, X. W., Dong, Z. Y., Long, X. Y., Li, S. F., Zuo, X. N., Zhu, C. Z., He, Y., Yan, C. G., and Zang, Y. F. (2011). REST: a toolkit for resting-state functional magnetic resonance imaging data processing. *PLoS One, 6*(9), e25031. doi: 10.1371/journal.pone.0025031

Sowell, E. R. (2004). Longitudinal Mapping of Cortical Thickness and Brain Growth in Normal Children. *Journal of Neuroscience, 24*(38), 8223-8231. doi: 10.1523/jneurosci.1798-04.2004

Vasios, C. E., Angelone, L. M., Purdon, P. L., Ahveninen, J., Belliveau, J. W., and Bonmassar, G. (2006). EEG/(f)MRI measurements at 7 Tesla using a new EEG cap ("InkCap"). *NeuroImage, 33*(4), 1082-1092. doi: 10.1016/j.neuroimage.2006.07.038

Yarnykh, V. L. (2007). Actual flip-angle imaging in the pulsed steady state: a method for rapid three-dimensional mapping of the transmitted radiofrequency field. *Magn Reson Med, 57*(1), 192-200. doi: 10.1002/mrm.21120

Highlights

- A high-density EEG cap leads to B_0 and B_1 field map inhomogeneities
- Perturbations of B_0 and B_1 field maps strongly influence morphometric measurements
- simultaneously recorded EEG-fMRI reveals reliable results for the T2*-weighted data